Model-independent measurement of mixing parameters in $D^0 \rightarrow K_S^0 \pi^+ \pi^-$ decays

The LHCb collaboration

E-mail: matthew.john.charles@cern.ch

ABSTRACT: The first model-independent measurement of the charm mixing parameters in the decay $D^0 \rightarrow K_S^0 \pi^+ \pi^-$ is reported, using a sample of pp collision data recorded by the LHCb experiment, corresponding to an integrated luminosity of $1.0\,\mathrm{fb}^{-1}$ at a centre-of-mass energy of $7\,\mathrm{TeV}$. The measured values are

$$x = (-0.86 \pm 0.53 \pm 0.17) \times 10^{-2},$$
$$y = (+0.03 \pm 0.46 \pm 0.13) \times 10^{-2},$$

where the first uncertainties are statistical and include small contributions due to the external input for the strong phase measured by the CLEO collaboration, and the second uncertainties are systematic.

Contents

1 Introduction

Mixing occurs in weakly decaying neutral mesons for which the flavour eigenstates of the particle and antiparticle (e.g. D^0 and $\overline{D}^0$) are not distinguished by any conserved quantum number. It is characterised by the differences in mass, ΔM, and width, $\Delta \Gamma$, between the mass eigenstates. In the charm system these are usually expressed in a reduced form, $x \equiv \Delta M/\Gamma$ and $y \equiv \Delta \Gamma/(2\Gamma)$, where Γ is the average of the two widths.

Mixing in charm has been observed with a significance above five standard deviations in several independent measurements [1–4] and the constraints on (x, y) are now rather precise [5]. However, most of the measurements are sensitive to $(x^2 + y^2)$ or to y (in the limit of negligible CP violation), leading to an ambiguity in the sign of x. One approach to resolve this ambiguity is to exploit the decay to the three-body, self-conjugate final state $D^0 \to K_S^0 \pi^+ \pi^-$ [6–8].

The advantage of decays such as $D^0 \to K_S^0 \pi^+ \pi^-$ is that both Cabibbo-favoured (CF) and doubly Cabibbo-suppressed (DCS) components are present in the same final state. Therefore the strong phase differences between contributing amplitudes — and hence between mixed and unmixed decays — can be measured with an amplitude analysis [7–10] of the same data sample used to obtain the mixing parameters. This is the approach that has

been used to date. A second method, proposed in ref. [11] and building upon a related approach for determining the unitarity triangle angle γ [12], uses measurements of the average strong phase difference in regions of the phase space. These can be obtained from an e^+e^- collider operating at the $\psi(3770)$ resonance. CLEO has made suitable measurements [13] and a similar study could be carried out with the larger BESIII [14] $\psi(3770)$ sample. The advantage of this second method is that no amplitude analysis is needed: the systematic uncertainty associated with the amplitude model is replaced with the uncertainty on the strong phase measurements. It has been estimated that with BESIII data this external uncertainty should be smaller than the statistical uncertainty for $D^0 \to K_S^0\pi^+\pi^-$ yields of up to 10–20 million [15], far larger than those available today. This paper describes the first measurement of x and y with this novel method, using promptly produced charm mesons in the decay chain $D^{*+} \to D^0\pi^+, D^0 \to K_S^0\pi^+\pi^-, K_S^0 \to \pi^+\pi^-$ (charge conjugate processes are included implicitly unless otherwise noted). A sample of pp collision data recorded by the LHCb experiment in 2011 is used, corresponding to an integrated luminosity of $1.0\,\mathrm{fb}^{-1}$ at a centre-of-mass energy of $7\,\mathrm{TeV}$.

2 Formalism

The formalism for the method has been presented previously [11, 13, 15], but is summarised here for clarity. The flavour eigenstates, $|D^0\rangle$ and $|\overline{D}^0\rangle$, are related to the mass eigenstates, $|D_1\rangle$ and $|D_2\rangle$, via

$$|D_1\rangle = p|D^0\rangle - q|\overline{D}^0\rangle, \tag{2.1}$$

$$|D_2\rangle = p|D^0\rangle + q|\overline{D}^0\rangle, \tag{2.2}$$

where $|p|^2 + |q|^2 = 1$. In the limit of CP conservation, $|p/q| = 1$. There is one free phase that is fixed by stipulating that in the limit of no indirect CP violation, $q/p = +1$ and $|D_1\rangle$ is the CP-odd eigenstate. The sign convention adopted for the mixing parameters is

$$x = (M_2 - M_1)/\Gamma, \tag{2.3}$$

$$y = (\Gamma_2 - \Gamma_1)/(2\Gamma). \tag{2.4}$$

For a state that is initially pure D^0 at $t = 0$, let the state at some later time t be $|D^0(t)\rangle$. Likewise, let the time evolution of $\overline{D}^0$ be $|\overline{D}^0(t)\rangle$. These may be evaluated as

$$|D^0(t)\rangle = g_+(t)|D^0\rangle + \frac{q}{p} g_-(t)|\overline{D}^0\rangle, \tag{2.5}$$

$$|\overline{D}^0(t)\rangle = \frac{p}{q} g_-(t)|D^0\rangle + g_+(t)|\overline{D}^0\rangle, \tag{2.6}$$

where

$$g_\pm(t) \equiv \frac{e^{-i(M_2 - i\Gamma_2/2)t} \pm e^{-i(M_1 - i\Gamma_1/2)t}}{2}. \tag{2.7}$$

The phase space for the three-body decay of a D^0 or $\overline{D}^0$ meson to $K_S^0\pi^+\pi^-$ is conventionally represented as a Dalitz plot and can be described by two variables, $m_{12}^2 =$

$m^2(K_{\mathrm{s}}^0 \pi^+)$ and $m_{13}^2 = m^2(K_{\mathrm{s}}^0 \pi^-)$. Let the amplitude for a D^0 decay to a point (m_{12}^2, m_{13}^2) in the phase space be $\mathcal{A}_{D^0}(m_{12}^2, m_{13}^2)$. Neglecting direct CP violation, the amplitudes for D^0 and $\overline{D}^0$ are related by the exchange $m_{12}^2 \leftrightarrow m_{13}^2$,

$$\mathcal{A}_{\overline{D}^0}(m_{12}^2, m_{13}^2) = \mathcal{A}_{D^0}(m_{13}^2, m_{12}^2). \tag{2.8}$$

In the expressions that follow, the explicit dependence of the amplitude terms $\mathcal{A}_{D^0}$ and $\mathcal{A}_{\overline{D}^0}$ on m_{12}^2 and m_{13}^2 is omitted. The amplitude $A_{D^0}(m_{12}^2, m_{13}^2, t)$ for a state that was initially D^0 to decay at some later time t to a point (m_{12}^2, m_{13}^2) in the phase space is

$$A_{D^0}(m_{12}^2, m_{13}^2, t) = \mathcal{A}_{D^0}\, g_+(t) + \frac{q}{p}\mathcal{A}_{\overline{D}^0}\, g_-(t). \tag{2.9}$$

Similarly,

$$A_{\overline{D}^0}(m_{12}^2, m_{13}^2, t) = \mathcal{A}_{\overline{D}^0}\, g_+(t) + \frac{p}{q}\mathcal{A}_{D^0}\, g_-(t). \tag{2.10}$$

The probability density $\mathcal{P}_{D^0}(m_{12}^2, m_{13}^2, t)$ is given by the modulus squared of the amplitude multiplied by a normalisation factor of Γ,

$$\mathcal{P}_{D^0}(m_{12}^2, m_{13}^2, t) = \Gamma \left| A_{D^0}(m_{12}^2, m_{13}^2, t) \right|^2, \tag{2.11}$$

with $\mathcal{P}_{\overline{D}^0}$ defined similarly in terms of $A_{\overline{D}^0}$. Performing a Taylor expansion and neglecting terms of order x^2, xy, and y^2, these evaluate to

$$\mathcal{P}_{D^0}(m_{12}^2, m_{13}^2, t) = \Gamma e^{-\Gamma t} \left[|\mathcal{A}_{D^0}|^2 - \Gamma t \, \mathrm{Re}\left(\frac{q}{p} \mathcal{A}_{D^0}^\star \mathcal{A}_{\overline{D}^0}(y + i\,x) \right) \right], \tag{2.12}$$

$$\mathcal{P}_{\overline{D}^0}(m_{12}^2, m_{13}^2, t) = \Gamma e^{-\Gamma t} \left[|\mathcal{A}_{\overline{D}^0}|^2 - \Gamma t \, \mathrm{Re}\left(\frac{p}{q} \mathcal{A}_{D^0} \mathcal{A}_{\overline{D}^0}^\star(y + i\,x) \right) \right]. \tag{2.13}$$

Neglecting CP violation for the purposes of the mixing measurement, $q/p = 1$ and hence

$$\mathcal{P}_{D^0}(m_{12}^2, m_{13}^2, t) = \Gamma e^{-\Gamma t} \left[|\mathcal{A}_{D^0}|^2 - \Gamma t \, \mathrm{Re}\left(\mathcal{A}_{D^0}^\star \mathcal{A}_{\overline{D}^0}(y + i\,x) \right) \right], \tag{2.14}$$

$$\mathcal{P}_{\overline{D}^0}(m_{12}^2, m_{13}^2, t) = \Gamma e^{-\Gamma t} \left[|\mathcal{A}_{\overline{D}^0}|^2 - \Gamma t \, \mathrm{Re}\left(\mathcal{A}_{\overline{D}^0} \mathcal{A}_{D^0}^\star(y + i\,x) \right) \right]. \tag{2.15}$$

These densities may be integrated over regions of the phase space. Various binning schemes are possible; this analysis uses the one referred to as the "equal $\Delta\delta_D$ BaBar 2008" binning in ref. [13], in which the strong phase variation within each bin of the phase space is minimised. This has the advantage of reducing the sensitivity to detector effects such as variation in efficiency across the phase space. In this scheme there are 16 bins, with bins 1 to 8 in the region of the phase space $m_{12}^2 > m_{13}^2$ and bins -1 to -8 in the region $m_{12}^2 < m_{13}^2$. The bins are symmetric about the leading diagonal, with bin i mapped to bin $-i$ by the transformation $(m_{12}^2, m_{13}^2) \to (m_{13}^2, m_{12}^2)$. The quantities T_i and X_i are defined by the integrals

$$T_i \equiv \int_i |\mathcal{A}_{D^0}|^2 \, \mathrm{d}m_{12}^2 \, \mathrm{d}m_{13}^2, \tag{2.16}$$

$$X_i \equiv \frac{1}{\sqrt{T_i T_{-i}}} \int_i \mathcal{A}_{D^0}^\star \, \mathcal{A}_{\overline{D}^0} \, \mathrm{d}m_{12}^2 \, \mathrm{d}m_{13}^2, \tag{2.17}$$

and the X_i may in turn be expressed in terms of real quantities c_i and s_i as

$$c_i \equiv \operatorname{Re}(X_i), \tag{2.18}$$

$$s_i \equiv -\operatorname{Im}(X_i). \tag{2.19}$$

Given the symmetric binning, eq. (2.8) implies that $X_{-i} = X_i^\star$, and thus $c_{-i} = c_i$ and $s_{-i} = -s_i$.

With these definitions, the integrated probability densities are

$$\begin{aligned}
\mathcal{P}_{D^0}(i;t) &= \int_i \mathcal{P}_{D^0}(m_{12}^2, m_{13}^2, t)\, \mathrm{d}m_{12}^2\, \mathrm{d}m_{13}^2 \\
&= \Gamma\, e^{-\Gamma t} \left[T_i - \Gamma t \sqrt{T_i T_{-i}} \left\{ y c_i + x s_i \right\} \right],
\end{aligned} \tag{2.20}$$

and

$$\mathcal{P}_{\bar{D}^0}(i;t) = \Gamma\, e^{-\Gamma t} \left[T_{-i} - \Gamma t \sqrt{T_i T_{-i}} \left\{ y c_i - x s_i \right\} \right]. \tag{2.21}$$

These distributions are used to obtain the mixing parameters x and y. The values of T_i, c_i, and s_i measured by the CLEO collaboration are given in tables VII and XVI of ref. [13].[1]

3 Detector, selection and simulation

The LHCb detector [16, 17] is a single-arm forward spectrometer covering the pseudo-rapidity range $2 < \eta < 5$, designed for the study of particles containing b or c quarks. The detector includes a high-precision tracking system consisting of a silicon-strip vertex detector surrounding the pp interaction region, a large-area silicon-strip detector located upstream of a dipole magnet with a bending power of about $4\,\mathrm{Tm}$, and three stations of silicon-strip detectors and straw drift tubes placed downstream of the magnet. The tracking system provides a measurement of momentum, p, of charged particles with a relative uncertainty that varies from 0.5% at low momentum to 1.0% at $200\,\mathrm{GeV}/c$. The minimum distance of a track to a primary vertex, the impact parameter (IP), is measured with a resolution of $(15 + 29/p_\mathrm{T})\,\mu\mathrm{m}$, where p_T is the component of the momentum transverse to the beam, in GeV/c. Different types of charged hadrons are distinguished using information from two ring-imaging Cherenkov detectors. Photons, electrons and hadrons are identified by a calorimeter system consisting of scintillating-pad and preshower detectors, an electromagnetic calorimeter and a hadronic calorimeter. Muons are identified by a system composed of alternating layers of iron and multiwire proportional chambers.

The online event selection is performed by a trigger [18], which consists of a hardware stage, based on information from the calorimeter and muon systems, followed by a software stage, which applies a full event reconstruction. At the hardware trigger stage, events are required to have a muon with high p_T or a hadron, photon or electron with high transverse energy in the calorimeters. In the subsequent software trigger, pairs of oppositely charged tracks are combined to form K_S^0 candidates, and those are in turn combined with a second pair of oppositely charged tracks to form D^0 candidates. For the 2011 dataset, the trigger

---

[1]Note that the captions for tables VII and VIII were exchanged in ref. [13], and that the supplementary material defining the binning contains an off-by-one error in the bin indices.

requires that all four tracks be reconstructed in the vertex detector, reducing the K_S^0 efficiency significantly. Both the K_S^0 and D^0 candidate vertices are required to be displaced from any primary pp interaction vertex (PV) in the event, and additional geometrical and kinematic critera are applied to suppress background and ensure consistency with a $D^0 \to K_S^0 \pi^+ \pi^-$ decay. These include a requirement that at least one of the four tracks has an impact parameter larger than $100\,\mu\text{m}$ with respect to any PV.

After offline processing, additional selection criteria are applied to further suppress background. These include particle identification requirements on the D^0 daughter tracks, as well as requirements that the track and vertex fits be of good quality, that the K_S^0 vertex be at least $10\,\text{mm}$ downstream of the D^0 vertex, that the K_S^0 candidate mass lie within $\pm 11.4\,\text{MeV}/c^2$ of the known value [19], that the D^0 candidate mass m_D lie within $\pm 85\,\text{MeV}/c^2$ of the known value [19], and that the reconstructed D^0 decay time t_D lie within $0.3 < t_D < 5\,\text{ps}$. The D^0 candidate is also required to have no more than two turning points in its decay time acceptance function (see section 4.3). It is then combined with a fifth pion track, referred to as the soft pion, to form a D^{*+} candidate. Both the soft pion and D^0 candidate are constrained to originate from the same PV. Good vertex fit quality is required, and particle identification requirements are applied to the soft pion. The mass difference $\Delta m = m_{D^{*+}} - m_D$ is required to lie within the range $m_\pi < \Delta m < (m_\pi + 15\,\text{MeV}/c^2)$, where $m_{D^{*+}}$ is the mass of the D^{*+} candidate and m_π is the charged pion mass. If there is more than one distinct $D^0 \to K_S^0 \pi^+ \pi^-$ candidate then one is chosen at random and the rest are discarded. If, after this, there are multiple $D^{*\pm}$ candidates then the one with the best vertex fit quality is retained and the rest are discarded.

Simulated events are used for cross-checks. In the simulation, pp collisions are generated using PYTHIA 6 [20] with a specific LHCb configuration [21]. Decays of hadronic particles are described by EVTGEN [22], in which final-state radiation is generated using PHOTOS [23]. The interaction of the generated particles with the detector, and its response, are implemented using the GEANT4 toolkit [24, 25] as described in ref. [26].

4 Fits

4.1 Overview

The mixing parameters x and y are determined by a sequence of fits to the distributions of the variables $(m_D, \Delta m)$ and $(t_D, \ln \chi_{\text{IP}}^2)$, initially in the whole phase space and later in individual regions. The impact parameter χ^2, χ_{IP}^2, is defined as the difference in the vertex fit χ^2 of the associated PV with and without the D^0 candidate. It is used to separate prompt charm that originates at the PV from secondary charm produced at a displaced vertex. The dominant source of secondary charm is from decays of b-hadrons. Two other variables are also used to describe the per-event decay time acceptance function, introduced in section 4.3. Unless otherwise specified, all data passing the selection described in section 3 are used. Where reference is made to a narrow signal window in m_D or Δm, this corresponds to a stricter requirement: $\pm 20\,\text{MeV}/c^2$ around the known D^0 mass, or $144.2 <$

$\Delta m < 146.4\,\text{MeV}/c^2$. The mass sidebands are defined as $1785 < m_D < 1810\,\text{MeV}/c^2$ and $1920 < m_D < 1945\,\text{MeV}/c^2$.

First, an extended maximum likelihood fit to the m_D distribution of all selected D^{*+} candidates is performed to determine the amounts of D^0 signal and combinatorial background in the narrow m_D signal window (section 4.2). Second is a maximum likelihood fit to the $(t_D, \ln \chi^2_{\text{IP}})$ distribution of those candidates in the narrow m_D signal window, using the mass sidebands to estimate the background distributions (section 4.4). This fit uses the yields determined in the first fit, and serves to determine the $\ln \chi^2_{\text{IP}}$ shapes for prompt and secondary charm. It is not sensitive to mixing. Third is a set of 32 extended maximum likelihood fits, each to the $(m_D, \Delta m)$ distribution in a particular phase space bin, with the D^{*+} and D^{*-} samples fitted separately (section 4.5). Each fit provides measurements of the amounts of signal and background in the narrow $(m_D, \Delta m)$ window for the corresponding bin. Fourth is a simultaneous maximum likelihood fit to the $(t_D, \ln \chi^2_{\text{IP}})$ distributions of candidates for the 32 subsamples (section 4.6). Signal candidates are required to lie in the narrow m_D and Δm signal windows, with the mass sidebands used to constrain the combinatorial background. This fit uses the $\ln \chi^2_{\text{IP}}$ shapes from the second fit and the yield estimates from the third fit, and produces measurements of the mixing parameters x and y.

Only the fit procedure and results are discussed in this section. Cross-checks and systematic uncertainties are discussed in section 5. All aspects of the selection and fit procedure were finalised before any measurements of x and y were made. Unless otherwise stated, all parameters introduced are left free in the fits.

4.2 Fit to m_D

The probability density functions (PDFs) used to model the m_D distributions are expressed in terms of exponential, Gaussian (G), bifurcated Gaussian (B), and Crystal Ball (C) [27] functions. Only two components are needed: D^0 signal and combinatorial background. The PDF for D^0 signal (sig) is the sum of a Gaussian, a bifurcated Gaussian, and a Crystal Ball function,

$$f_1(m_D|\text{sig}) = \eta_1\, G(m_D; \mu_D, \sigma_1) + \eta_2\, B(m_D; \mu_D, \sigma_L, \sigma_R) + (1 - \eta_1 - \eta_2)\, C(m_D; \mu_D, \sigma_2, \alpha, n),$$
$$(4.1)$$

where the order of the Crystal Ball function, n, is fixed to three. The PDF for the combinatorial background, $f_1(m_D|\text{cmb})$, is an exponential function. The total PDF is then

$$f_1(m_D) = P_1(\text{sig})\, f_1(m_D|\text{sig}) + P_1(\text{cmb})\, f_1(m_D|\text{cmb}), \qquad (4.2)$$

where $P_1(\text{sig})$ and $P_1(\text{cmb})$ describe the fractions of signal and background in the data sample used for the first fit, and sum to unity.

The results of the first fit are shown in figure 1. The fit yields 178k signal events within the narrow m_D signal window, and the purity within this window is $(97.4 \pm 0.3)\%$.

4.3 Time acceptance correction

The probability for a D^{*+} signal decay to be successfully triggered, reconstructed, and selected depends upon the decay time of its D^0 daughter. The time-dependent fits must,
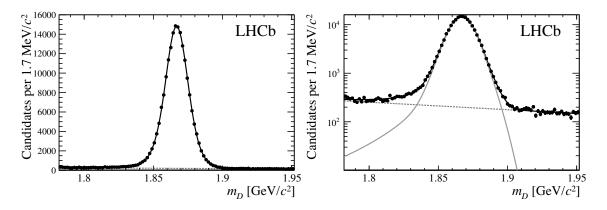
Figure 1. Fitted m_D distribution. Both plots show the same data sample with (left) linear and (right) logarithmic vertical scales. The curves show the results of the first fit, described in section 4.2: the total (solid black), the background component (dotted), and the signal component (grey, right only).

therefore, take account of the nonuniform decay time acceptance. A data-driven method referred to as swimming [28] is used. This approach follows that used in previous LHCb measurements of the mixing and indirect CP violation parameters, y_{CP} and A_Γ, in D^0 decays [29, 30], and at previous experiments [31–34].

The principle of the method is that the decay time acceptance is determined by selection criteria that can be reproduced later. The criteria for this analysis are given in section 3. (In practice they are applied to the measured rather than the true decay time; the resolution is neglected and considered as a systematic effect (section 5).) Those criteria can be tested again after modifying the candidate — specifically, with a different decay time. By repeatedly testing the criteria for many decay time values spanning the allowed range, the acceptance function for an individual candidate may be determined empirically. Aside from a correction factor discussed later in this section, the value of this function is 1 for those decay times at which all of the criteria are fulfilled, and 0 at all other times. Since candidates with $t_D < 0.3\,\mathrm{ps}$ are rejected, the acceptance function is zero below that point. It must also be zero at very large decay times, both because of the upper bound on t_D and because of the finite length of the vertex detector. Therefore, the acceptance function will take the form of a top-hat function $[\Theta(t_D - t_0) - \Theta(t_D - t_1)]$, where Θ is the Heaviside function and $t_1 > t_0$, or will be the sum of several nonoverlapping top-hat functions. The decay times at which the acceptance changes between 0 and 1 are referred to as the turning points.

For approximately 90% of selected candidates, the acceptance is a single top-hat with exactly two turning points. The remaining candidates have a more complicated acceptance function, typically due to the presence of a second pp primary vertex nearby. As in the previous analysis using this technique [30], candidates with more than two turning points are rejected. This enables a more robust description of the turning point variable distributions (see below) and suppresses events in which the primary vertex association is ambiguous.

The implementation of the decay time acceptance calculation is simplified by a number of assumptions. First, the hardware triggers do not depend on the D^0 decay time and can

therefore be ignored when evaluating the acceptance function. Second, the decay time acceptance depends only on the D^0 reconstruction and selection: it is not affected by the soft pion and D^{*+} requirements. Third, the full vertex detector pattern recognition is not re-run when changing the D^0 decay time; instead, the changes to the decay geometry are made analytically. Requirements on the number of hits on a track in the vertex detector subsystem are approximated as requirements that the modified trajectory pass through a corresponding number of subdetector modules. Finally, an additional correction factor $\varepsilon(t_D)$ is applied to the acceptance function to model the effect of a track quality cut in the reconstruction, which reduces the efficiency for tracks produced further from the beam axis. The correction is derived from samples of simulated events and is parameterised as a polynomial function.

For an individual event, the acceptance function can be written as

$$a(t_D; t_0, \Delta t) = [\Theta(t_D - t_0) - \Theta(t_D - t_0 - \Delta t)]\, \varepsilon(t_D), \tag{4.3}$$

where t_0 is the first turning point (TP) and Δt is the difference between the two turning points. Although the acceptance function is determined for each event independently, models of the distribution $f_{\mathrm{TP}}(t_0, \Delta t)$ of the turning point variables t_0 and Δt are required for the decay time fits. The distribution is assumed to factorise,

$$f_{\mathrm{TP}}(t_0, \Delta t) = f_{\mathrm{TP},0}(t_0)\, f_{\mathrm{TP},\Delta}(\Delta t). \tag{4.4}$$

Nonparametric functions are used to model the turning point PDFs. The distribution $f_{\mathrm{TP},0}(t_0)$ is modelled as a histogram PDF with 100 bins spanning the range 0–3 ps and the distribution $f_{\mathrm{TP},\Delta}(\Delta t)$ is modelled as a one-dimensional Gaussian kernel PDF [35]. The same method is used for all components, and is based on data in the mass sidebands for combinatorial background. Candidates in the narrow mass signal window are used for prompt and secondary D^0 mesons, both of which are assumed to have the same turning point distribution in the baseline fit.

4.4 Separation of prompt and secondary candidates

The second fit is used to determine the relative proportions of prompt and secondary D^0 signal, and to model their $\ln \chi^2_{\mathrm{IP}}$ distributions. It also serves as an important cross-check since it allows the mean D^0 lifetime to be computed in the $D^0 \to K^0_S \pi^+ \pi^-$ sample. No distinction is made in the fit between D^0 and $\overline{D}^0$ candidates, nor between different regions of the phase space, so by design it is insensitive to mixing. While a dominance of CP-odd or of CP-even components in the final state could in principle shift the mean lifetime by up to $\pm y\,\Gamma \approx 2.5$ fs, the net CP has recently been shown to be almost zero [36] so that the effective lifetime is close to τ_D. Similarly, previous amplitude analyses all found that the decay is dominated by flavour-specific processes, with total fit fractions of about 70% [7–10], implying that the maximum scale of the effect is below the sensitivity of this analysis.

In this fit, the underlying decay time distribution for the prompt (prm) D^0 signal is taken to be an exponential function for $t_D > 0$ with characteristic time τ_D. For a

particular event, the expected t_D distribution is this exponential multiplied by the per-event acceptance function given in eq. (4.3),

$$f_2(t_D|t_0, \Delta t; \mathrm{prm}) = n \, a(t_D; t_0, \Delta t) \, e^{-t_D/\tau_D}, \qquad (4.5)$$

where n is a normalisation factor and the decay time resolution has been neglected. Note that the expression in eq. (4.5) depends explicitly on the turning point variables t_0 and Δt. To separate out this dependence, the models for the turning point distributions given in section 4.3 are used. The PDF for prompt charm may then be written as

$$\begin{aligned} f_2(t_0, \Delta t, t_D, \ln \chi_{\mathrm{IP}}^2 | \mathrm{prm}) &= f_2(\ln \chi_{\mathrm{IP}}^2 | t_D; \mathrm{prm}) \, f_2(t_D|t_0, \Delta t; \mathrm{prm}) \\ &\quad \times f_{\mathrm{TP},0}(t_0|D) \, f_{\mathrm{TP},\Delta}(\Delta t|D), \end{aligned} \qquad (4.6)$$

where D denotes PDFs used for both prompt and secondary D^0, and $f_2(\ln \chi_{\mathrm{IP}}^2 | t_D; \mathrm{prm})$ is a parameterisation of the $\ln \chi_{\mathrm{IP}}^2$ distribution for a given decay time, taking the form

$$f_2(\ln \chi_{\mathrm{IP}}^2 | t_D; \mathrm{prm}) = \eta \, G(\ln \chi_{\mathrm{IP}}^2; \mu_{\mathrm{p}}(t_D), \sigma_1) + (1 - \eta) \, B(\ln \chi_{\mathrm{IP}}^2; \mu_{\mathrm{p}}(t_D), \sigma_L, \sigma_R), \qquad (4.7)$$

where $\mu_{\mathrm{p}}(t_D)$, the most probable value of $\ln \chi_{\mathrm{IP}}^2$, is a linear function.

A similar approach is used for the secondary (sec) D^0 signal, except that the underlying decay time distribution is taken to be the convolution of two exponential functions restricted to $t_D > 0$ and with characteristic times τ_1 and τ_2. Since $\left[\Theta(t_D) \, e^{-t_D/\tau_1}\right] \otimes \left[\Theta(t_D) \, e^{-t_D/\tau_2}\right]$ may be rewritten as $(e^{-t_D/\tau_2} - e^{-t_D/\tau_1})$ with an appropriate normalisation factor, the expression remains analytically integrable and takes the form

$$f_2(t_D|t_0, \Delta t; \mathrm{sec}) = n \, a(t_D; t_0, \Delta t) \, \left(e^{-t_D/\tau_2} - e^{-t_D/\tau_1} \right), \qquad (4.8)$$

where n is again a normalisation factor. The $\ln \chi_{\mathrm{IP}}^2$ distribution also differs from that used for prompt charm,

$$f_2(\ln \chi_{\mathrm{IP}}^2 | t_D; \mathrm{sec}) = \eta \, G(\ln \chi_{\mathrm{IP}}^2; \mu_{\mathrm{s}}(t_D), \alpha \, \sigma_1) + (1 - \eta) \, B(\ln \chi_{\mathrm{IP}}^2; \mu_{\mathrm{s}}(t_D), \alpha \, (\sigma_L + \beta t_D), \alpha \, \sigma_R). \qquad (4.9)$$

Compared to eq. (4.7), the width of the peak is multiplied by α, with the lower tail of the bifurcated Gaussian having a further, time-dependent broadening. In addition, the decay time at which the function is maximised, $\mu_{\mathrm{s}}(t_D)$, is taken empirically to evolve as

$$\mu_{\mathrm{s}}(t_D) = \mu_{\mathrm{s}0} + B(1 - e^{Ct_D}). \qquad (4.10)$$

Using the models for the turning point distributions given in section 4.3, the PDF for secondary charm may be written as

$$\begin{aligned} f_2(t_0, \Delta t, t_D, \ln \chi_{\mathrm{IP}}^2 | \mathrm{sec}) &= f_2(\ln \chi_{\mathrm{IP}}^2 | t_D; \mathrm{sec}) \, f_2(t_D|t_0, \Delta t; \mathrm{sec}) \\ &\quad \times f_{\mathrm{TP},0}(t_0|D) \, f_{\mathrm{TP},\Delta}(\Delta t|D). \end{aligned} \qquad (4.11)$$

The combinatorial background is described in a different way. To begin, a nonparametric distribution is fitted to the data in the mass sidebands. However, this model, a two-dimensional Gaussian kernel function, cannot be used directly in the fit: the PDF

used must depend explicitly on the turning point variables [37]. Therefore, an unfolding procedure is applied to obtain the underlying decay time distribution before acceptance effects. The acceptance is then incorporated in the same way as for the other components. The PDF for combinatorial background may be written as

$$f_2(t_0, \Delta t, t_D, \ln \chi^2_{\text{IP}}|\text{cmb}) = f_2(\ln \chi^2_{\text{IP}}|t_D; \text{cmb}) \, f_2(t_D|t_0, \Delta t; \text{cmb})$$
$$\times f_{\text{TP},0}(t_0|\text{cmb}) \, f_{\text{TP},\Delta}(\Delta t|\text{cmb}), \tag{4.12}$$

where $f_{\text{TP},0}(t_0|\text{cmb})$ and $f_{\text{TP},\Delta}(\Delta t|\text{cmb})$ are obtained as described in section 4.3, and $f_2(\ln \chi^2_{\text{IP}}|t_D; \text{cmb})$ and $f_2(t_D|t_0, \Delta t; \text{cmb})$ are derived from the distributions in the mass sidebands as described above.

Combining the above, the total PDF used in the fit is

$$f_2(t_0, \Delta t, t_D, \ln \chi^2_{\text{IP}}) = \sum_j f_2(t_0, \Delta t, t_D, \ln \chi^2_{\text{IP}}|j) P_2(j), \tag{4.13}$$

where the index j runs over the prompt, secondary, and combinatoric components and $\sum_j P_2(j) = 1$. The value of $P_2(\text{cmb})$ is fixed based on the results of the preceeding fit to m_D. The sum $[P_2(\text{prm}) + P_2(\text{sec})]$ is likewise fixed, but with the secondary fraction of the signal free.

Pseudoexperiments are used to validate the fit procedure. In each pseudoexperiment, events from each category (prompt D^0 mesons, secondary D^0 mesons, and combinatorial background) are generated according to the expected distributions and analysed following the same procedure as used for data, including estimation of the per-event decay time acceptance function with the swimming method. In an ensemble of approximately 500 pseudoexperiments generated assuming a true D^0 lifetime of 410 ps, the mean of the fitted values of τ_D is 409.92 ± 0.06 fs, and the normalised residuals are described by a Gaussian distribution with a mean of 0.016 ± 0.049 and a width of 1.03 ± 0.04.

Applying the fit to the data, the measured lifetime is $\tau_D = 410.9 \pm 1.1$ fs, where the uncertainty is purely statistical. This is consistent with the world average value of 410.1 ± 1.5 fs [19]. The agreement between the fit and data is shown in figure 2. An excess is seen at very long decay times, likely due to imperfect modelling of the secondary component, but there is no effect on the measurement of the lifetime of the prompt component.

4.5 Fits to m_D and Δm

The third step consists of separate fits to the $(m_D, \Delta m)$ distributions of the phase space bins. The fits include three components: D^{*+} signal (sig), background from genuine D^0 that are combined with an unrelated soft pion (Dbg), and combinatorial background (cmb). In each case, the PDF is assumed to factorise into m_D-dependent and Δm-dependent terms. The three components may be written as

$$f_3(m_D, \Delta m|\text{sig}) = f_3(m_D|\text{peak}) \, f_3(\Delta m|\text{peak}), \tag{4.14}$$
$$f_3(m_D, \Delta m|\text{Dbg}) = f_3(m_D|\text{peak}) \, f_3(\Delta m|\text{smooth}), \tag{4.15}$$
$$f_3(m_D, \Delta m|\text{cmb}) = f_3(m_D|\text{smooth}) \, f_3(\Delta m|\text{smooth}), \tag{4.16}$$
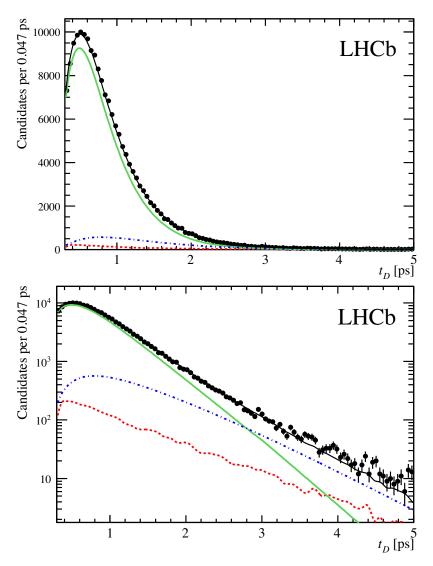
Figure 2. Decay time projection from the fit for separation of prompt and secondary candidates. The curves show the results of the fit described in section 4.4: the total (solid black), the prompt component (solid green), the secondary component (dot-dashed blue), and the combinatorial component (dashed red). Both plots show the same data sample with linear (top) and logarithmic (bottom) vertical scales.

where the peaking components are defined as

$$f_3(m_D|\text{peak}) = \eta_1 G(m_D; \mu_D, \sigma_1) + \eta_2 G(m_D; \mu_D, \sigma_2)$$
$$+ (1 - \eta_1 - \eta_2) C(m_D; \mu_D, \sigma_3, \alpha, n), \tag{4.17}$$

$$f_3(\Delta m|\text{peak}) = \eta_3 G(\Delta m; \mu_{\Delta m}, \sigma_4) + \eta_4 G(\Delta m; \mu_{\Delta m}, \sigma_5)$$
$$+ (1 - \eta_3 - \eta_4) B(\Delta m; \mu_{\Delta m}, \sigma_L, \sigma_R). \tag{4.18}$$

For the nonpeaking components, $f_3(m_D|\text{smooth})$ is an exponential function and $f_3(\Delta m|\text{smooth})$ is a second-order polynomial. The total PDF may then be written as

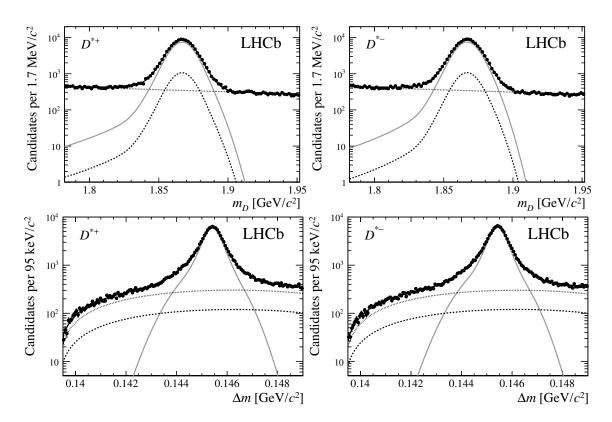$$f_3(m_D, \Delta m) = \sum_j f_3(m_D, \Delta m|j) P_3(j), \tag{4.19}$$

Figure 3. Fitted $(m_D, \Delta m)$ distributions. The upper row shows the m_D projection and the lower row Δm. The left column shows D^{*+} candidates and the right column D^{*-}. The signal and background components are shown separately (signal as solid grey, D^0 background dashed, combinatoric background dotted, and the sum as solid black).

where the index j runs over the signal, D^0 background, and combinatoric components, and $\sum_j P_3(j) = 1$.

To avoid an excessive number of free parameters when splitting the data into many independent subsamples, the third fit is done in two stages. Initially, fits to $f_3(m_D, \Delta m)$ are done without dividing the data by phase space bin such that there are only two subsamples, D^{*+} and D^{*-}. The results of these fits are shown in figure 3 and correspond to yields of approximately 85k each of D^{*+} and D^{*-} within the narrow signal window. The parameters for $f_3(m_D|\text{peak})$, $f_3(\Delta m|\text{peak})$, and $f_3(\Delta m|\text{smooth})$ are then fixed. Individual fits to each of the 32 subsamples are then carried out, with only the parameters of the combinatorial background shape, $f_3(m_D|\text{smooth})$, and the yield fractions $P_3(j)$ free.

4.6 Mixing parameters

The fourth fit uses the $(t_D, \ln \chi^2_{\text{IP}})$ distributions in each of the phase space bins for D^0 and $\overline{D}^0$ to determine the mixing parameters x and y. For a particular phase space bin i and $D^{*\pm}$ charge q, the total PDF is

$$f_4(t_0, \Delta t, t_D, \ln \chi^2_{\text{IP}}, i, q) = \sum_j f_4(t_0, \Delta t, t_D, \ln \chi^2_{\text{IP}}, i, q|j)P_4(i, q, j), \qquad (4.20)$$

where $\sum_j P_4(i, q, j) = 1$ and the index j runs over the components: prompt $D^{*\pm}$ (p-sig), prompt D^0 background (p-Dbg), secondary $D^{*\pm}$ (s-sig), secondary D^0 background (s-Dbg), and combinatorial background (cmb).

The prompt $D^{*\pm}$ component comprises prompt D^0 or $\overline{D}^0$ mesons whose initial flavour is correctly identified. Its underlying decay time distribution is given by $\mathcal{P}_{D^0}(i; t_D)$ in eq. (2.20) for D^{*+} and by $\mathcal{P}_{\overline{D}^0}(i; t_D)$ in eq. (2.21) for D^{*-}, denoted $\mathcal{P}_q$. Taking the time-dependent acceptance into account in the same way as was done for the second fit in eq. (4.5), the per-candidate decay time PDF is

$$f_4(t_D|t_0, \Delta t, i, q; \text{p-sig}) = n\, a(t_D; t_0, \Delta t)\, \mathcal{P}_q(i; t_D), \tag{4.21}$$

where n is a normalisation constant. The $\ln \chi^2_{\text{IP}}$ distribution for prompt D^{*+} signal at a given decay time is fixed to that obtained in the second fit (see eq. (4.7)), as is that for prompt D^0 background,

$$f_4(\ln \chi^2_{\text{IP}}|t_D; \text{p-sig}) = f_4(\ln \chi^2_{\text{IP}}|t_D; \text{p-Dbg}) = f_2(\ln \chi^2_{\text{IP}}|t_D; \text{prm}). \tag{4.22}$$

The non-parametric turning point distributions, $f_{\text{TP},0}(t_0|i; D)$ and $f_{\text{TP},\Delta}(\Delta t|i; D)$, are obtained in the same way as was done for the second fit, except that each phase space bin is now considered separately; here the label D denotes that the distributions are used for all components that contain a real D^0 or $\overline{D}^0$ (p-sig, p-Dbg, s-sig, s-Dbg). The prompt D^{*+} PDF is

$$\begin{aligned} f_4(t_0, \Delta t, t_D, \ln \chi^2_{\text{IP}}, i, q|\text{p-sig}) = {} & f_4(\ln \chi^2_{\text{IP}}|t_D; \text{p-sig})\, f_4(t_D|t_0, \Delta t, i, q; \text{p-sig}) \\ & \times f_{\text{TP},0}(t_0|i; D)\, f_{\text{TP},\Delta}(\Delta t|i; D). \end{aligned} \tag{4.23}$$

The prompt D^0 background component consists of correctly reconstructed prompt D^0 (or $\overline{D}^0$) mesons, each of which is paired with an unrelated soft pion such that the assigned initial flavour is random. Ignoring the assigned flavour, the underlying decay time distribution for phase space bin i, $u(t_D; i)$, is a linear combination of $\mathcal{P}_{D^0}(i; t_D)$ and $\mathcal{P}_{\overline{D}^0}(i; t_D)$. The coefficients depend on the relative populations of bin i for D^0 and bin $-i$ for $\overline{D}^0$, T_i and T_{-i} defined in eq. (2.16), since the $\overline{D}^0$ Dalitz plot is the mirror reflection of that of D^0 neglecting CP violation. The underlying decay time distribution is thus

$$u(t_D; i) = \frac{p_{D^0} T_i \mathcal{P}_{D^0}(i; t_D) + (1 - p_{D^0}) T_{-i} \mathcal{P}_{\overline{D}^0}(i; t_D)}{p_{D^0} T_i + (1 - p_{D^0}) T_{-i}}, \tag{4.24}$$

where p_{D^0} is the fraction of the prompt D^0 background due to D^0 mesons and $(1 - p_{D^0})$ is the fraction due to $\overline{D}^0$ mesons. Since production and detection charge asymmetries for pions in the relevant kinematic region are small [38], p_{D^0} is assumed to be 0.5. The per-candidate decay time PDF is then

$$f_4(t_D|t_0, \Delta t, i, q; \text{p-Dbg}) = n\, a(t_D; t_0, \Delta t)\, u(t_D; i), \tag{4.25}$$

where n is again a calculable normalisation factor. The turning point distributions $f_{\text{TP},0}(t_0|\text{prompt})$ and $f_{\text{TP},\Delta}(\Delta t|\text{prompt})$ are fixed to be the same as those obtained in

the second fit. The prompt D^0 background PDF is

$$f_4(t_0, \Delta t, t_D, \ln \chi^2_{\text{IP}}, i, q|\text{p-Dbg}) = f_4(\ln \chi^2_{\text{IP}}|t_D; \text{p-Dbg}) \, f_4(t_D|t_0, \Delta t, i, q; \text{p-Dbg}) \\ \times \, f_{\text{TP},0}(t_0|i; D) \, f_{\text{TP},\Delta}(\Delta t|i; D). \tag{4.26}$$

For the secondary $D^{*\pm}$ and secondary D^0 background components, the effect of mixing is neglected so that the underlying time distribution does not depend on the identified flavour or on the phase space bin. The same functional form is used as for the second fit, and the parameters are fixed to those obtained in the second fit. Thus, the PDF is the same as that given in eq. (4.11),

$$f_4(t_0, \Delta t, t_D, \ln \chi^2_{\text{IP}}, i, q|\text{s-sig}) = f_4(t_0, \Delta t, t_D, \ln \chi^2_{\text{IP}}, i, q|\text{s-Dbg}) = f_2(t_0, \Delta t, t_D, \ln \chi^2_{\text{IP}}|\text{sec}). \tag{4.27}$$

It is assumed that the fraction of $D^{*\pm}$ signal that is from secondary production is the same in every phase space bin, and that the same fraction also applies to the secondary D^0 background.

For the combinatorial component, nonparametric models are used for the decay time and $\ln \chi^2_{\text{IP}}$ distributions in a similar way to the second fit. However, the distributions for each of the 32 subsamples, split by phase space bin and by $D^{*\pm}$ charge, are modelled independently according to the mass sidebands for that bin and charge.

Thus, nearly all of the parameters in the total PDF for the fourth fit (eq. (4.20)) are fixed. Likewise, the fractions for each component $P_4(i, q, j)$ are fixed based on the previous fits. The T_i values are fixed to those obtained by CLEO (so as to reduce the number of free parameters and improve fit behaviour). The only free parameters are x, y, $\Gamma_D = 1/\tau_D$, and the set of (c_i, s_i) values. For the latter, the information on the CLEO measurements and their uncertainties, including correlations, is incorporated as a set of correlated Gaussian constraints on the likelihood.

As in section 4.4, pseudoexperiments are used to validate the fit procedure, following all steps including the per-event decay time acceptance determination. An ensemble of 1000 experiments is generated with `cfit` [39] taking $\Gamma_D = 2.44 \, \text{ps}^{-1}$, $x = -1 \times 10^{-2}$, and $y = +1 \times 10^{-2}$. The mean fitted values of x and y are found to differ from the input values by $(-0.016 \pm 0.014) \times 10^{-2}$ and $(+0.013 \pm 0.016) \times 10^{-2}$, respectively. The mean fitted value of Γ_D differs from the input value by $(+0.0012 \pm 0.0002) \, \text{ps}^{-1}$; although this indicates a measureable bias, it is only approximately one sixth the size of the statistical uncertainty on Γ_D. Since Γ_D is measured here only as a cross-check, this is ignored. Validation tests are also performed with a sample of pseudoevents generated with Pythia and EvtGen, corresponding to approximately double the yield in data, and with a sample of events in which the full detector response was simulated with Geant4, corresponding to approximately a quarter of the yield in data. The output is consistent with the input values of the mixing parameters supplied to the generators.

The results of the fit to data are

$$x = (-0.86 \pm 0.53) \times 10^{-2},$$
$$y = (+0.03 \pm 0.46) \times 10^{-2},$$
$$\Gamma_D = 2.435 \pm 0.006 \, \text{ps}^{-1}.$$

The correlation coefficient between x and y is $+0.37$. The uncertainties quoted above are the statistical uncertainties estimated by the likelihood fit. They do not include any systematic effects, but they do implicitly include the propagated uncertainties on the CLEO (c_i, s_i) parameters. These are estimated with pseudoexperiments to be in the range $(0.05$–$0.15) \times 10^{-2}$. As a check, the fit to data is repeated with the (c_i, s_i) values fixed to those obtained by CLEO, giving $x = (-0.73 \pm 0.48) \times 10^{-2}$ and $y = (+0.05 \pm 0.45) \times 10^{-2}$, with Γ_D unchanged. The shifts in x and y are consistent with the uncertainties associated with the CLEO parameters.

5 Systematic uncertainties

Further cross-checks are performed and systematic effects considered, as summarised in table 1. Several sources of systematic uncertainty are due to assumptions made for the baseline fit procedure. These uncertainties are estimated with ensembles of pseudoexperiments in which events are generated so as to mimic the effect being studied. For these tests, the systematic uncertainties on x and y are typically estimated as the sum in quadrature of the shift in the central value and the uncertainty on the shift. The fit procedure was also validated with a sample of events in which the detector response was simulated using GEANT4 as outlined in section 3; the values of x and y obtained were consistent with the input parameters.

Biases on x and y due to the fit procedure itself are assessed through the use of pseudoexperiments. The resolutions on the decay time, on the turning points, and on m_{12}^2 and m_{13}^2 are evaluated by generating pseudoexperiments with resolution smearing and then fitting them with the baseline procedure in which the resolution is neglected. Estimates of the resolutions are taken from data or from the full simulation based on GEANT4. The assumption that the turning point distributions of prompt and secondary signal are equivalent is tested with pseudoexperiments in which these distributions are drawn from prompt-enriched ($\ln \chi_{\mathrm{IP}}^2 < 1$) and secondary-enriched ($\ln \chi_{\mathrm{IP}}^2 > 3$) samples, respectively. The impact of neglecting variation in efficiency as a function of position in the Dalitz plot is assessed by generating pseudoexperiments with a nonuniform efficiency model, determined with full simulation, and fitting them with the baseline procedure. The efficiency is described by a polynomial function and the following variations are tested: the order of the polynomial, whether or not it is required to be symmetric about the leading diagonal in the Dalitz plot, and the use of a different event selection. The variation among models in the values of x and y is smaller than the systematic uncertainties quoted, which are based on the variation with respect to the baseline fit; in particular, the variation in x among the models is approximately 0.01×10^{-2}. The uncertainty associated with the model of the tracking efficiency correction $\varepsilon(t_D)$, discussed in section 4.3, is assessed by allowing higher-order terms in the model. Due to the absence of a K_{S}^0 mass constraint, a small fraction of events fall outside the expected Dalitz plot boundary in the baseline procedure and an algorithm is used to assign them to a nearby bin; the effect of this is tested by instead rejecting all such events. To test the modelling of the combinatorial background,

Source	$x\,(\times 10^{-2})$	$y\,(\times 10^{-2})$
Fit bias	0.021	0.020
Decay time resolution	0.065	0.039
Turning point (TP) resolution	0.020	0.022
Invariant mass resolution	0.073	0.028
Prompt/secondary TP distributions	0.051	0.023
Efficiency over phase space	0.057	0.071
Tracking efficiency parameterisation	0.015	0.025
Kinematic boundary	0.012	0.006
Combinatorial background	0.061	0.052
Treatment of secondary D decays	0.046	0.025
Uncertainty from T_i	0.079	0.056
Uncertainties from $(m_D, \Delta m)$ fits	0.000	0.000
Uncertainties from lifetime fit	0.020	0.043
D^0 background	0.001	0.006
Variation of signal components across the phase space	0.013	0.017
Total systematic uncertainty	0.171	0.134
Statistical uncertainty	0.527	0.463

Table 1. Systematic uncertainties on x and y. The statistical uncertainties, which include the uncertainties associated with the CLEO parameters (c_i, s_i), are shown for comparison.

the procedure is repeated using just the data in one of the two sidebands, with the D^{*+} and D^{*-} samples separated (as in the baseline fit) or combined.

In addition, the uncertainties associated with a number of parameters that are fixed in the baseline fit are included, generally by rerunning the baseline fit repeatedly with the parameters fixed to different values obtained by smearing the nominal values randomly according to their estimated uncertainties. This procedure is used for the T_i values from CLEO, for the yield fractions estimated from the third fit to the $(m_D, \Delta m)$ distribution, and for the decay time and $\ln \chi^2_{\rm IP}$ parameters fixed based on the second fit. The effects of varying the D^0-$\overline{D}^0$ composition of the prompt D^0 background (via the fraction p_{D^0}) and of using separate models of the prompt and secondary $\ln \chi^2_{\rm IP}$ distributions for each phase space bin are also tested.

The sum in quadrature of the systematic uncertainties is 0.17×10^{-2} for x and 0.13×10^{-2} for y.

6 Conclusions

The charm mixing parameters x and y have been measured using a novel method that does not require the use of an amplitude model but instead uses external measurements

of the strong phase made at an e^+e^- collider running at the $\psi(3770)$ resonance [13]. A sample of pp collision data recorded by the LHCb experiment was used, corresponding to an integrated luminosity of $1.0\,\text{fb}^{-1}$ at a centre-of-mass energy of $7\,\text{TeV}$. Neglecting CP violation, the measured values are

$$x = (-0.86 \pm 0.53 \pm 0.17) \times 10^{-2},$$
$$y = (+0.03 \pm 0.46 \pm 0.13) \times 10^{-2}.$$

The first uncertainties are combinations of the LHCb statistical uncertainties and those due to the CLEO measurements of the (c_i, s_i) parameters, whose effect is too small to determine precisely from the fit but is estimated to be in the range $(0.05\text{–}0.15) \times 10^{-2}$. The second uncertainties are systematic. The correlation coefficient between x and y for the first uncertainty is $+0.37$, and the systematic uncertainties are considered uncorrelated. The analysis prefers a negative value of x, but positive values are not excluded. The current HFAG world averages [5] are $x = (+0.37 \pm 0.16) \times 10^{-2}$ and $y = (+0.66\,^{+0.07}_{-0.10}) \times 10^{-2}$.

This analysis constitutes a proof of principle that the mixing parameters can be measured in $D^0 \to K_{\mathrm{S}}^0 \pi^+\pi^-$ decays at LHCb without the need for an amplitude model. The statistical uncertainty will be be reduced substantially by the addition of the 2012 data sample due to improvements in the software trigger, which now accepts $D^0 \to K_{\mathrm{S}}^0 \pi^+\pi^-$ decays in which the K_{S}^0 vertex lies outside the vertex detector, as occurs in the majority of cases. A further improvement may be obtained if charm mesons produced in semileptonic b-hadron decays are incorporated. The method does not require a detailed model of the efficiency as a function of position in the phase space, and the decay time acceptance is determined from data. Thus, the method does not rely on the extensive use of Monte Carlo simulation. This is crucial for future analyses, especially in the context of the planned LHCb upgrade where $\mathcal{O}(10^8)$ signal events are expected [40]. To take full advantage of such a data set, more precise strong phase measurements from a charm factory running on the $\psi(3770)$ resonance will be needed.

Acknowledgments

References

[1] LHCb collaboration, *Observation of $D^0 - \overline{D}^0$ oscillations*, *Phys. Rev. Lett.* **110** (2013) 101802 [arXiv:1211.1230] [INSPIRE].

[2] CDF collaboration, T.A. Aaltonen et al., *Observation of $D^0 - \overline{D}^0$ Mixing Using the CDF II Detector*, *Phys. Rev. Lett.* **111** (2013) 231802 [arXiv:1309.4078] [INSPIRE].

[3] LHCb collaboration, *Measurement of $D^0 - \overline{D}^0$ Mixing Parameters and Search for CP Violation Using $D^0 \to K^+\pi^-$ Decays*, *Phys. Rev. Lett.* **111** (2013) 251801 [arXiv:1309.6534] [INSPIRE].

[4] BELLE collaboration, B.R. Ko et al., *Observation of $D^0 - \overline{D}^0$ Mixing in e^+e^- Collisions*, *Phys. Rev. Lett.* **112** (2014) 111801 [arXiv:1401.3402] [INSPIRE].

[5] HEAVY FLAVOR AVERAGING GROUP (HFAG) collaboration, Y. Amhis et al., *Averages of b-hadron, c-hadron and τ-lepton properties as of summer 2014*, arXiv:1412.7515 [INSPIRE] and updated results and plots available at http://www.slac.stanford.edu/xorg/hfag/.

[6] CLEO collaboration, D.M. Asner et al., *Search for $D^0 - \overline{D}^0$ mixing in the Dalitz plot analysis of $D^0 \to K^0_S\pi^+\pi^-$*, *Phys. Rev.* **D 72** (2005) 012001 [hep-ex/0503045] [INSPIRE].

[7] BaBar collaboration, P. del Amo Sanchez et al., *Measurement of $D^0 - \overline{D}^0$ mixing parameters using $D^0 \to K^0_S\pi^+\pi^-$ and $D^0 \to K^0_S K^+K^-$ decays*, *Phys. Rev. Lett.* **105** (2010) 081803 [arXiv:1004.5053] [INSPIRE].

[8] BELLE collaboration, T. Peng et al., *Measurement of $D^0 - \overline{D}^0$ mixing and search for indirect CP-violation using $D^0 \to K^0_S\pi^+\pi^-$ decays*, *Phys. Rev.* **D 89** (2014) 091103 [arXiv:1404.2412] [INSPIRE].

[9] CLEO collaboration, H. Muramatsu et al., *Dalitz analysis of $D^0 \to K^0_S\pi^+\pi^-$*, *Phys. Rev. Lett.* **89** (2002) 251802 [*Erratum ibid.* **90** (2003) 059901] [hep-ex/0207067] [INSPIRE].

[10] CDF collaboration, T.A. Aaltonen et al., *Measurement of CP-violation asymmetries in $D^0 \to K_S\pi^+\pi^-$*, *Phys. Rev.* **D 86** (2012) 032007 [arXiv:1207.0825] [INSPIRE].

[11] A. Bondar, A. Poluektov and V. Vorobiev, *Charm mixing in the model-independent analysis of correlated $D^0\overline{D}^0$ decays*, *Phys. Rev.* **D 82** (2010) 034033 [arXiv:1004.2350] [INSPIRE].

[12] A. Giri, Y. Grossman, A. Soffer and J. Zupan, *Determining γ using $B^\pm \to DK^\pm$ with multibody D decays*, *Phys. Rev.* **D 68** (2003) 054018 [hep-ph/0303187] [INSPIRE].

[13] CLEO collaboration, J. Libby et al., *Model-independent determination of the strong-phase difference between D^0 and $\overline{D}^0 \to K^0_{S,L} h^+ h^-$ ($h = \pi, K$) and its impact on the measurement of the CKM angle γ/ϕ_3*, *Phys. Rev.* **D 82** (2010) 112006 [arXiv:1010.2817] [INSPIRE].

[14] BESIII collaboration, M. Ablikim et al., *Design and Construction of the BESIII Detector*, *Nucl. Instrum. Meth.* **A 614** (2010) 345 [arXiv:0911.4960] [INSPIRE].

[15] C. Thomas and G. Wilkinson, *Model-independent $D^0 - \overline{D}^0$ mixing and CP-violation studies with $D^0 \to K^0_S \pi^+ \pi^-$ and $D^0 \to K^0_S K^+ K^-$*, *JHEP* **10** (2012) 185 [arXiv:1209.0172] [INSPIRE].

[16] LHCb collaboration, *The LHCb Detector at the LHC*, 2008 *JINST* **3** S08005 [INSPIRE].

[17] LHCb collaboration, *LHCb Detector Performance*, *Int. J. Mod. Phys.* **A 30** (2015) 1530022 [arXiv:1412.6352] [INSPIRE].

[18] R. Aaij et al., *The LHCb Trigger and its Performance in 2011*, 2013 *JINST* **8** P04022 [arXiv:1211.3055] [INSPIRE].

[19] PARTICLE DATA GROUP collaboration, K.A. Olive et al., *Review of Particle Physics*, *Chin. Phys.* **C 38** (2014) 090001 [INSPIRE].

[20] T. Sjöstrand, S. Mrenna and P.Z. Skands, *PYTHIA 6.4 Physics and Manual*, *JHEP* **05** (2006) 026 [hep-ph/0603175] [INSPIRE].

[21] LHCb collaboration, *Handling of the generation of primary events in Gauss, the LHCb simulation framework*, *J. Phys. Conf. Ser.* **331** (2011) 032047 [INSPIRE].

[22] D.J. Lange, *The EvtGen particle decay simulation package*, *Nucl. Instrum. Meth.* **A 462** (2001) 152 [INSPIRE].

[23] P. Golonka and Z. Was, *PHOTOS Monte Carlo: A Precision tool for QED corrections in Z and W decays*, *Eur. Phys. J.* **C 45** (2006) 97 [hep-ph/0506026] [INSPIRE].

[24] GEANT4 collaboration, J. Allison et al., *Geant4 developments and applications*, *IEEE Trans. Nucl. Sci.* **53** (2006) 270 [INSPIRE].

[25] GEANT4 collaboration, S. Agostinelli et al., *GEANT4: A Simulation toolkit*, *Nucl. Instrum. Meth.* **A 506** (2003) 250 [INSPIRE].

[26] LHCb collaboration, *The LHCb simulation application, Gauss: Design, evolution and experience*, *J. Phys. Conf. Ser.* **331** (2011) 032023 [INSPIRE].

[27] T. Skwarnicki, *A study of the radiative cascade transitions between the Upsilon-prime and Upsilon resonances*, Ph.D. Thesis, Institute of Nuclear Physics, Krakow (1986) [DESY-F31-86-02] [INSPIRE].

[28] V.V. Gligorov et al., *Swimming: A data driven acceptance correction algorithm*, *J. Phys. Conf. Ser.* **396** (2012) 022016 [INSPIRE].

[29] LHCb collaboration, *Measurement of mixing and CP-violation parameters in two-body charm decays*, *JHEP* **04** (2012) 129 [arXiv:1112.4698] [INSPIRE].

[30] LHCb collaboration, *Measurements of indirect CP asymmetries in $D^0 \to K^- K^+$ and $D^0 \to \pi^- \pi^+$ decays*, *Phys. Rev. Lett.* **112** (2014) 041801 [arXiv:1310.7201] [INSPIRE].

[31] NA11 collaboration, R. Bailey et al., *Measurement of the lifetime of charged and neutral D mesons with high resolution silicon strip detectors*, *Z. Phys.* **C 28** (1985) 357 [INSPIRE].

[32] DELPHI collaboration, W. Adam et al., *Lifetimes of charged and neutral B hadrons using event topology*, *Z. Phys.* **C 68** (1995) 363 [ɪɴSPIRE].

[33] J. Rademacker, *Reduction of statistical power per event due to upper lifetime cuts in lifetime measurements*, *Nucl. Instrum. Meth.* **A 570** (2007) 525 [hep-ex/0502042] [ɪɴSPIRE].

[34] CDF collaboration, T.A. Aaltonen et al., *Measurement of the B^- lifetime using a simulation free approach for trigger bias correction*, *Phys. Rev.* **D 83** (2011) 032008 [arXiv:1004.4855] [ɪɴSPIRE].

[35] D. Scott, *Multivariate density estimation: Theory, practice, and visualization*, John Wiley and Sons, Inc. (1992).

[36] T. Gershon, J. Libby and G. Wilkinson, *Contributions to the width difference in the neutral D system from hadronic decays*, *Phys. Lett.* **B 750** (2015) 338 [arXiv:1506.08594] [ɪɴSPIRE].

[37] G. Punzi, *Comments on likelihood fits with variable resolution*, *eConf* **C 030908** (2003) WELT002 [physics/0401045] [ɪɴSPIRE].

[38] LHCb collaboration, *Measurement of the $D_s^+ - D_s^-$ production asymmetry in 7 TeV pp collisions*, *Phys. Lett.* **B 713** (2012) 186 [arXiv:1205.0897] [ɪɴSPIRE].

[39] J. Garra Tico, *The cfit fitting package*, http://www.github.com/cfit.

[40] LHCb collaboration, *Implications of LHCb measurements and future prospects*, *Eur. Phys. J.* **C 73** (2013) 2373 [arXiv:1208.3355] [ɪɴSPIRE].

JHEP04(2016)033

The LHCb collaboration

R. Aaij[38], C. Abellán Beteta[40], B. Adeva[37], M. Adinolfi[46], A. Affolder[52], Z. Ajaltouni[5], S. Akar[6],
J. Albrecht[9], F. Alessio[38], M. Alexander[51], S. Ali[41], G. Alkhazov[30], P. Alvarez Cartelle[53],
A.A. Alves Jr[57], S. Amato[2], S. Amerio[22], Y. Amhis[7], L. An[3], L. Anderlini[17], J. Anderson[40],
G. Andreassi[39], M. Andreotti[16,f], J.E. Andrews[58], R.B. Appleby[54], O. Aquines Gutierrez[10],
F. Archilli[38], P. d'Argent[11], A. Artamonov[35], M. Artuso[59], E. Aslanides[6], G. Auriemma[25,m],
M. Baalouch[5], S. Bachmann[11], J.J. Back[48], A. Badalov[36], C. Baesso[60], W. Baldini[16,38],
R.J. Barlow[54], C. Barschel[38], S. Barsuk[7], W. Barter[38], V. Batozskaya[28], V. Battista[39], A. Bay[39],
L. Beaucourt[4], J. Beddow[51], F. Bedeschi[23], I. Bediaga[1], L.J. Bel[41], V. Bellee[39], N. Belloli[20,j],
I. Belyaev[31], E. Ben-Haim[8], G. Bencivenni[18], S. Benson[38], J. Benton[46], A. Berezhnoy[32],
R. Bernet[40], A. Bertolin[22], M.-O. Bettler[38], M. van Beuzekom[41], A. Bien[11], S. Bifani[45],
P. Billoir[8], T. Bird[54], A. Birnkraut[9], A. Bizzeti[17,h], T. Blake[48], F. Blanc[39], J. Blouw[10],
S. Blusk[59], V. Bocci[25], A. Bondar[34], N. Bondar[30,38], W. Bonivento[15], S. Borghi[54], M. Borsato[7],
T.J.V. Bowcock[52], E. Bowen[40], C. Bozzi[16], S. Braun[11], M. Britsch[10], T. Britton[59], J. Brodzicka[54],
N.H. Brook[46], E. Buchanan[46], C. Burr[54], A. Bursche[40], J. Buytaert[38], S. Cadeddu[15],
R. Calabrese[16,f], M. Calvi[20,j], M. Calvo Gomez[36,o], P. Campana[18], D. Campora Perez[38],
L. Capriotti[54], A. Carbone[14,d], G. Carboni[24,k], R. Cardinale[19,i], A. Cardini[15], P. Carniti[20,j],
L. Carson[50], K. Carvalho Akiba[2,38], G. Casse[52], L. Cassina[20,j], L. Castillo Garcia[38],
M. Cattaneo[38], Ch. Cauet[9], G. Cavallero[19], R. Cenci[23,s], M. Charles[8], Ph. Charpentier[38],
M. Chefdeville[4], S. Chen[54], S.-F. Cheung[55], N. Chiapolini[40], M. Chrzaszcz[40], X. Cid Vidal[38],
G. Ciezarek[41], P.E.L. Clarke[50], M. Clemencic[38], H.V. Cliff[47], J. Closier[38], V. Coco[38], J. Cogan[6],
E. Cogneras[5], V. Cogoni[15,e], L. Cojocariu[29], G. Collazuol[22], P. Collins[38], A. Comerma-Montells[11],
A. Contu[15], A. Cook[46], M. Coombes[46], S. Coquereau[8], G. Corti[38], M. Corvo[16,f], B. Couturier[38],
G.A. Cowan[50], D.C. Craik[48], A. Crocombe[48], M. Cruz Torres[60], S. Cunliffe[53], R. Currie[53],
C. D'Ambrosio[38], E. Dall'Occo[41], J. Dalseno[46], P.N.Y. David[41], A. Davis[57],
O. De Aguiar Francisco[2], K. De Bruyn[6], S. De Capua[54], M. De Cian[11], J.M. De Miranda[1],
L. De Paula[2], P. De Simone[18], C.-T. Dean[51], D. Decamp[4], M. Deckenhoff[9], L. Del Buono[8],
N. Déléage[4], M. Demmer[9], D. Derkach[65], O. Deschamps[5], F. Dettori[38], B. Dey[21], A. Di Canto[38],
F. Di Ruscio[24], H. Dijkstra[38], S. Donleavy[52], F. Dordei[11], M. Dorigo[39], A. Dosil Suárez[37],
D. Dossett[48], A. Dovbnya[43], K. Dreimanis[52], L. Dufour[41], G. Dujany[54], F. Dupertuis[39],
P. Durante[38], R. Dzhelyadin[35], A. Dziurda[26], A. Dzyuba[30], S. Easo[49,38], U. Egede[53],
V. Egorychev[31], S. Eidelman[34], S. Eisenhardt[50], U. Eitschberger[9], R. Ekelhof[9], L. Eklund[51],
I. El Rifai[5], Ch. Elsasser[40], S. Ely[59], S. Esen[11], H.M. Evans[47], T. Evans[55], A. Falabella[14],
C. Färber[38], N. Farley[45], S. Farry[52], R. Fay[52], D. Ferguson[50], V. Fernandez Albor[37], F. Ferrari[14],
F. Ferreira Rodrigues[1], M. Ferro-Luzzi[38], S. Filippov[33], M. Fiore[16,38,f], M. Fiorini[16,f],
M. Firlej[27], C. Fitzpatrick[39], T. Fiutowski[27], K. Fohl[38], P. Fol[53], M. Fontana[15], F. Fontanelli[19,i],
D. C. Forshaw[59], R. Forty[38], M. Frank[38], C. Frei[38], M. Frosini[17], J. Fu[21], E. Furfaro[24,k],
A. Gallas Torreira[37], D. Galli[14,d], S. Gallorini[22], S. Gambetta[50], M. Gandelman[2], P. Gandini[55],
Y. Gao[3], J. García Pardiñas[37], J. Garra Tico[47], L. Garrido[36], D. Gascon[36], C. Gaspar[38],
R. Gauld[55], L. Gavardi[9], G. Gazzoni[5], D. Gerick[11], E. Gersabeck[11], M. Gersabeck[54],
T. Gershon[48], Ph. Ghez[4], S. Gianì[39], V. Gibson[47], O.G. Girard[39], L. Giubega[29], V.V. Gligorov[38],
C. Göbel[60], D. Golubkov[31], A. Golutvin[53,38], A. Gomes[1,a], C. Gotti[20,j], M. Grabalosa Gándara[5],
R. Graciani Diaz[36], L.A. Granado Cardoso[38], E. Graugés[36], E. Graverini[40], G. Graziani[17],
A. Grecu[29], E. Greening[55], S. Gregson[47], P. Griffith[45], L. Grillo[11], O. Grünberg[63], B. Gui[59],
E. Gushchin[33], Yu. Guz[35,38], T. Gys[38], T. Hadavizadeh[55], C. Hadjivasiliou[59], G. Haefeli[39],
C. Haen[38], S.C. Haines[47], S. Hall[53], B. Hamilton[58], X. Han[11], S. Hansmann-Menzemer[11],
N. Harnew[55], S.T. Harnew[46], J. Harrison[54], J. He[38], T. Head[39], V. Heijne[41], K. Hennessy[52],
P. Henrard[5], L. Henry[8], E. van Herwijnen[38], M. Heß[63], A. Hicheur[2], D. Hill[55], M. Hoballah[5],

C. Hombach[54], W. Hulsbergen[41], T. Humair[53], N. Hussain[55], D. Hutchcroft[52], D. Hynds[51],
M. Idzik[27], P. Ilten[56], R. Jacobsson[38], A. Jaeger[11], J. Jalocha[55], E. Jans[41], A. Jawahery[58],
F. Jing[3], M. John[55], D. Johnson[38], C.R. Jones[47], C. Joram[38], B. Jost[38], N. Jurik[59],
S. Kandybei[43], W. Kanso[6], M. Karacson[38], T.M. Karbach[38,†], S. Karodia[51], M. Kecke[11],
M. Kelsey[59], I.R. Kenyon[45], M. Kenzie[38], T. Ketel[42], E. Khairullin[65], B. Khanji[20,38,j],
C. Khurewathanakul[39], S. Klaver[54], K. Klimaszewski[28], O. Kochebina[7], M. Kolpin[11],
I. Komarov[39], R.F. Koopman[42], P. Koppenburg[41,38], M. Kozeiha[5], L. Kravchuk[33], K. Kreplin[11],
M. Kreps[48], G. Krocker[11], P. Krokovny[34], F. Kruse[9], W. Krzemien[28], W. Kucewicz[26,n],
M. Kucharczyk[26], V. Kudryavtsev[34], A. K. Kuonen[39], K. Kurek[28], T. Kvaratskheliya[31],
D. Lacarrere[38], G. Lafferty[54,38], A. Lai[15], D. Lambert[50], G. Lanfranchi[18], C. Langenbruch[48],
B. Langhans[38], T. Latham[48], C. Lazzeroni[45], R. Le Gac[6], J. van Leerdam[41], J.-P. Lees[4],
R. Lefèvre[5], A. Leflat[32,38], J. Lefrançois[7], E. Lemos Cid[37], O. Leroy[6], T. Lesiak[26],
B. Leverington[11], Y. Li[7], T. Likhomanenko[65,64], M. Liles[52], R. Lindner[38], C. Linn[38],
F. Lionetto[40], B. Liu[15], X. Liu[3], D. Loh[48], I. Longstaff[51], J.H. Lopes[2], D. Lucchesi[22,q],
M. Lucio Martinez[37], H. Luo[50], A. Lupato[22], E. Luppi[16,f], O. Lupton[55], A. Lusiani[23],
F. Machefert[7], F. Maciuc[29], O. Maev[30], K. Maguire[54], S. Malde[55], A. Malinin[64], G. Manca[7],
G. Mancinelli[6], P. Manning[59], A. Mapelli[38], J. Maratas[5], J.F. Marchand[4], U. Marconi[14],
C. Marin Benito[36], P. Marino[23,38,s], J. Marks[11], G. Martellotti[25], M. Martin[6], M. Martinelli[39],
D. Martinez Santos[37], F. Martinez Vidal[66], D. Martins Tostes[2], A. Massafferri[1], R. Matev[38],
A. Mathad[48], Z. Mathe[38], C. Matteuzzi[20], A. Mauri[40], B. Maurin[39], A. Mazurov[45],
M. McCann[53], J. McCarthy[45], A. McNab[54], R. McNulty[12], B. Meadows[57], F. Meier[9],
M. Meissner[11], D. Melnychuk[28], M. Merk[41], E Michielin[22], D.A. Milanes[62], M.-N. Minard[4],
D.S. Mitzel[11], J. Molina Rodriguez[60], I.A. Monroy[62], S. Monteil[5], M. Morandin[22], P. Morawski[27],
A. Mordà[6], M.J. Morello[23,s], J. Moron[27], A.B. Morris[50], R. Mountain[59], F. Muheim[50],
D. Müller[54], J. Müller[9], K. Müller[40], V. Müller[9], M. Mussini[14], B. Muster[39], P. Naik[46],
T. Nakada[39], R. Nandakumar[49], A. Nandi[55], I. Nasteva[2], M. Needham[50], N. Neri[21], S. Neubert[11],
N. Neufeld[38], M. Neuner[11], A.D. Nguyen[39], T.D. Nguyen[39], C. Nguyen-Mau[39,p], V. Niess[5],
R. Niet[9], N. Nikitin[32], T. Nikodem[11], A. Novoselov[35], D.P. O'Hanlon[48], A. Oblakowska-Mucha[27],
V. Obraztsov[35], S. Ogilvy[51], O. Okhrimenko[44], R. Oldeman[15,e], C.J.G. Onderwater[67],
B. Osorio Rodrigues[1], J.M. Otalora Goicochea[2], A. Otto[38], P. Owen[53], A. Oyanguren[66],
A. Palano[13,c], F. Palombo[21,t], M. Palutan[18], J. Panman[38], A. Papanestis[49], M. Pappagallo[51],
L.L. Pappalardo[16,f], C. Pappenheimer[57], W. Parker[58], C. Parkes[54], G. Passaleva[17], G.D. Patel[52],
M. Patel[53], C. Patrignani[19,i], A. Pearce[54,49], A. Pellegrino[41], G. Penso[25,l], M. Pepe Altarelli[38],
S. Perazzini[14,d], P. Perret[5], L. Pescatore[45], K. Petridis[46], A. Petrolini[19,i], M. Petruzzo[21],
E. Picatoste Olloqui[36], B. Pietrzyk[4], T. Pilař[48], D. Pinci[25], A. Pistone[19], A. Piucci[11],
S. Playfer[50], M. Plo Casasus[37], T. Poikela[38], F. Polci[8], A. Poluektov[48,34], I. Polyakov[31],
E. Polycarpo[2], A. Popov[35], D. Popov[10,38], B. Popovici[29], C. Potterat[2], E. Price[46], J.D. Price[52],
J. Prisciandaro[37], A. Pritchard[52], C. Prouve[46], V. Pugatch[44], A. Puig Navarro[39], G. Punzi[23,r],
W. Qian[4], R. Quagliani[7,46], B. Rachwal[26], J.H. Rademacker[46], M. Rama[23], M.S. Rangel[2],
I. Raniuk[43], N. Rauschmayr[38], G. Raven[42], F. Redi[53], S. Reichert[54], M.M. Reid[48], A.C. dos Reis[1],
S. Ricciardi[49], S. Richards[46], M. Rihl[38], K. Rinnert[52,38], V. Rives Molina[36], P. Robbe[7,38],
A.B. Rodrigues[1], E. Rodrigues[54], J.A. Rodriguez Lopez[62], P. Rodriguez Perez[54], S. Roiser[38],
V. Romanovsky[35], A. Romero Vidal[37], J. W. Ronayne[12], M. Rotondo[22], J. Rouvinet[39], T. Ruf[38],
P. Ruiz Valls[66], J.J. Saborido Silva[37], N. Sagidova[30], P. Sail[51], B. Saitta[15,e],
V. Salustino Guimaraes[2], C. Sanchez Mayordomo[66], B. Sanmartin Sedes[37], R. Santacesaria[25],
C. Santamarina Rios[37], M. Santimaria[18], E. Santovetti[24,k], A. Sarti[18,l], C. Satriano[25,m],
A. Satta[24], D.M. Saunders[46], D. Savrina[31,32], M. Schiller[38], H. Schindler[38], M. Schlupp[9],
M. Schmelling[10], T. Schmelzer[9], B. Schmidt[38], O. Schneider[39], A. Schopper[38], M. Schubiger[39],
M.-H. Schune[7], R. Schwemmer[38], B. Sciascia[18], A. Sciubba[25,l], A. Semennikov[31], N. Serra[40],

J. Serrano[6], L. Sestini[22], P. Seyfert[20], M. Shapkin[35], I. Shapoval[16,43,f], Y. Shcheglov[30],
T. Shears[52], L. Shekhtman[34], V. Shevchenko[64], A. Shires[9], B.G. Siddi[16], R. Silva Coutinho[40],
L. Silva de Oliveira[2], G. Simi[22], M. Sirendi[47], N. Skidmore[46], T. Skwarnicki[59], E. Smith[55,49],
E. Smith[53], I.T. Smith[50], J. Smith[47], M. Smith[54], H. Snoek[41], M.D. Sokoloff[57,38], F.J.P. Soler[51],
F. Soomro[39], D. Souza[46], B. Souza De Paula[2], B. Spaan[9], P. Spradlin[51], S. Sridharan[38],
F. Stagni[38], M. Stahl[11], S. Stahl[38], S. Stefkova[53], O. Steinkamp[40], O. Stenyakin[35], S. Stevenson[55],
S. Stoica[29], S. Stone[59], B. Storaci[40], S. Stracka[23,s], M. Straticiuc[29], U. Straumann[40], L. Sun[57],
W. Sutcliffe[53], K. Swientek[27], S. Swientek[9], V. Syropoulos[42], M. Szczekowski[28], T. Szumlak[27],
S. T'Jampens[4], A. Tayduganov[6], T. Tekampe[9], M. Teklishyn[7], G. Tellarini[16,f], F. Teubert[38],
C. Thomas[55], E. Thomas[38], J. van Tilburg[41], V. Tisserand[4], M. Tobin[39], J. Todd[57], S. Tolk[42],
L. Tomassetti[16,f], D. Tonelli[38], S. Topp-Joergensen[55], N. Torr[55], E. Tournefier[4], S. Tourneur[39],
K. Trabelsi[39], M.T. Tran[39], M. Tresch[40], A. Trisovic[38], A. Tsaregorodtsev[6], P. Tsopelas[41],
N. Tuning[41,38], A. Ukleja[28], A. Ustyuzhanin[65,64], U. Uwer[11], C. Vacca[15,38,e], V. Vagnoni[14],
G. Valenti[14], A. Vallier[7], R. Vazquez Gomez[18], P. Vazquez Regueiro[37], C. Vázquez Sierra[37],
S. Vecchi[16], J.J. Velthuis[46], M. Veltri[17,g], G. Veneziano[39], M. Vesterinen[11], B. Viaud[7], D. Vieira[2],
M. Vieites Diaz[37], X. Vilasis-Cardona[36,o], V. Volkov[32], A. Vollhardt[40], D. Volyanskyy[10],
D. Voong[46], A. Vorobyev[30], V. Vorobyev[34], C. Voß[63], J.A. de Vries[41], R. Waldi[63], C. Wallace[48],
R. Wallace[12], J. Walsh[23], S. Wandernoth[11], J. Wang[59], D.R. Ward[47], N.K. Watson[45],
D. Websdale[53], A. Weiden[40], M. Whitehead[48], G. Wilkinson[55,38], M. Wilkinson[59], M. Williams[38],
M.P. Williams[45], M. Williams[56], T. Williams[45], F.F. Wilson[49], J. Wimberley[58], J. Wishahi[9],
W. Wislicki[28], M. Witek[26], G. Wormser[7], S.A. Wotton[47], K. Wyllie[38], Y. Xie[61], Z. Xu[39],
Z. Yang[3], J. Yu[61], X. Yuan[34], O. Yushchenko[35], M. Zangoli[14], M. Zavertyaev[10,b], L. Zhang[3],
Y. Zhang[3], A. Zhelezov[11], A. Zhokhov[31], L. Zhong[3], S. Zucchelli[14].

1   Centro Brasileiro de Pesquisas Físicas (CBPF), Rio de Janeiro, Brazil
2   Universidade Federal do Rio de Janeiro (UFRJ), Rio de Janeiro, Brazil
3   Center for High Energy Physics, Tsinghua University, Beijing, China
4   LAPP, Université Savoie Mont-Blanc, CNRS/IN2P3, Annecy-Le-Vieux, France
5   Clermont Université, Université Blaise Pascal, CNRS/IN2P3, LPC, Clermont-Ferrand, France
6   CPPM, Aix-Marseille Université, CNRS/IN2P3, Marseille, France
7   LAL, Université Paris-Sud, CNRS/IN2P3, Orsay, France
8   LPNHE, Université Pierre et Marie Curie, Université Paris Diderot, CNRS/IN2P3, Paris, France
9   Fakultät Physik, Technische Universität Dortmund, Dortmund, Germany
10   Max-Planck-Institut für Kernphysik (MPIK), Heidelberg, Germany
11   Physikalisches Institut, Ruprecht-Karls-Universität Heidelberg, Heidelberg, Germany
12   School of Physics, University College Dublin, Dublin, Ireland
13   Sezione INFN di Bari, Bari, Italy
14   Sezione INFN di Bologna, Bologna, Italy
15   Sezione INFN di Cagliari, Cagliari, Italy
16   Sezione INFN di Ferrara, Ferrara, Italy
17   Sezione INFN di Firenze, Firenze, Italy
18   Laboratori Nazionali dell'INFN di Frascati, Frascati, Italy
19   Sezione INFN di Genova, Genova, Italy
20   Sezione INFN di Milano Bicocca, Milano, Italy
21   Sezione INFN di Milano, Milano, Italy
22   Sezione INFN di Padova, Padova, Italy
23   Sezione INFN di Pisa, Pisa, Italy
24   Sezione INFN di Roma Tor Vergata, Roma, Italy
25   Sezione INFN di Roma La Sapienza, Roma, Italy
26   Henryk Niewodniczanski Institute of Nuclear Physics Polish Academy of Sciences, Kraków, Poland

27 *AGH - University of Science and Technology, Faculty of Physics and Applied Computer Science, Kraków, Poland*

28 *National Center for Nuclear Research (NCBJ), Warsaw, Poland*

29 *Horia Hulubei National Institute of Physics and Nuclear Engineering, Bucharest-Magurele, Romania*

30 *Petersburg Nuclear Physics Institute (PNPI), Gatchina, Russia*

31 *Institute of Theoretical and Experimental Physics (ITEP), Moscow, Russia*

32 *Institute of Nuclear Physics, Moscow State University (SINP MSU), Moscow, Russia*

33 *Institute for Nuclear Research of the Russian Academy of Sciences (INR RAN), Moscow, Russia*

34 *Budker Institute of Nuclear Physics (SB RAS) and Novosibirsk State University, Novosibirsk, Russia*

35 *Institute for High Energy Physics (IHEP), Protvino, Russia*

36 *Universitat de Barcelona, Barcelona, Spain*

37 *Universidad de Santiago de Compostela, Santiago de Compostela, Spain*

38 *European Organization for Nuclear Research (CERN), Geneva, Switzerland*

39 *Ecole Polytechnique Fédérale de Lausanne (EPFL), Lausanne, Switzerland*

40 *Physik-Institut, Universität Zürich, Zürich, Switzerland*

41 *Nikhef National Institute for Subatomic Physics, Amsterdam, The Netherlands*

42 *Nikhef National Institute for Subatomic Physics and VU University Amsterdam, Amsterdam, The Netherlands*

43 *NSC Kharkiv Institute of Physics and Technology (NSC KIPT), Kharkiv, Ukraine*

44 *Institute for Nuclear Research of the National Academy of Sciences (KINR), Kyiv, Ukraine*

45 *University of Birmingham, Birmingham, United Kingdom*

46 *H.H. Wills Physics Laboratory, University of Bristol, Bristol, United Kingdom*

47 *Cavendish Laboratory, University of Cambridge, Cambridge, United Kingdom*

48 *Department of Physics, University of Warwick, Coventry, United Kingdom*

49 *STFC Rutherford Appleton Laboratory, Didcot, United Kingdom*

50 *School of Physics and Astronomy, University of Edinburgh, Edinburgh, United Kingdom*

51 *School of Physics and Astronomy, University of Glasgow, Glasgow, United Kingdom*

52 *Oliver Lodge Laboratory, University of Liverpool, Liverpool, United Kingdom*

53 *Imperial College London, London, United Kingdom*

54 *School of Physics and Astronomy, University of Manchester, Manchester, United Kingdom*

55 *Department of Physics, University of Oxford, Oxford, United Kingdom*

56 *Massachusetts Institute of Technology, Cambridge, MA, United States*

57 *University of Cincinnati, Cincinnati, OH, United States*

58 *University of Maryland, College Park, MD, United States*

59 *Syracuse University, Syracuse, NY, United States*

60 *Pontifícia Universidade Católica do Rio de Janeiro (PUC-Rio), Rio de Janeiro, Brazil, associated to [2]*

61 *Institute of Particle Physics, Central China Normal University, Wuhan, Hubei, China, associated to [3]*

62 *Departamento de Fisica , Universidad Nacional de Colombia, Bogota, Colombia, associated to [8]*

63 *Institut für Physik, Universität Rostock, Rostock, Germany, associated to [11]*

64 *National Research Centre Kurchatov Institute, Moscow, Russia, associated to [31]*

65 *Yandex School of Data Analysis, Moscow, Russia, associated to [31]*

66 *Instituto de Fisica Corpuscular (IFIC), Universitat de Valencia-CSIC, Valencia, Spain, associated to [36]*

67 *Van Swinderen Institute, University of Groningen, Groningen, The Netherlands, associated to [41]*

a *Universidade Federal do Triângulo Mineiro (UFTM), Uberaba-MG, Brazil*

b *P.N. Lebedev Physical Institute, Russian Academy of Science (LPI RAS), Moscow, Russia*

c *Università di Bari, Bari, Italy*

d *Università di Bologna, Bologna, Italy*

^{e} *Università di Cagliari, Cagliari, Italy*

^{f} *Università di Ferrara, Ferrara, Italy*

^{g} *Università di Urbino, Urbino, Italy*

^{h} *Università di Modena e Reggio Emilia, Modena, Italy*

^{i} *Università di Genova, Genova, Italy*

^{j} *Università di Milano Bicocca, Milano, Italy*

^{k} *Università di Roma Tor Vergata, Roma, Italy*

^{l} *Università di Roma La Sapienza, Roma, Italy*

^{m} *Università della Basilicata, Potenza, Italy*

^{n} *AGH - University of Science and Technology, Faculty of Computer Science, Electronics and Telecommunications, Kraków, Poland*

^{o} *LIFAELS, La Salle, Universitat Ramon Llull, Barcelona, Spain*

^{p} *Hanoi University of Science, Hanoi, Viet Nam*

^{q} *Università di Padova, Padova, Italy*

^{r} *Università di Pisa, Pisa, Italy*

^{s} *Scuola Normale Superiore, Pisa, Italy*

^{t} *Università degli Studi di Milano, Milano, Italy*

† *Deceased*